Systematic Degradation Analysis in Renewable Energy-Powered Proton Exchange Membrane Water Electrolysis

Anastasiia Voronova,[a,b] Sol Kim,[a,b] Dongwon Kim,[a] Hee-Young Park,[a] Jong Hyun Jang,[a,b] and Bora Seo[a,b,*]

[a] Hydrogen and Fuel Cell Research Center, Korea Institute of Science and Technology (KIST), 5 Hwarang-ro 14-gil, Seongbuk-gu, Seoul 02792, Republic of Korea.

[b] Division of Energy & Environment Technology, KIST School, University of Science and Technology (UST), Seoul 02792, Republic of Korea.

* *E-mail address*: brseo@kist.re.kr (B. Seo)
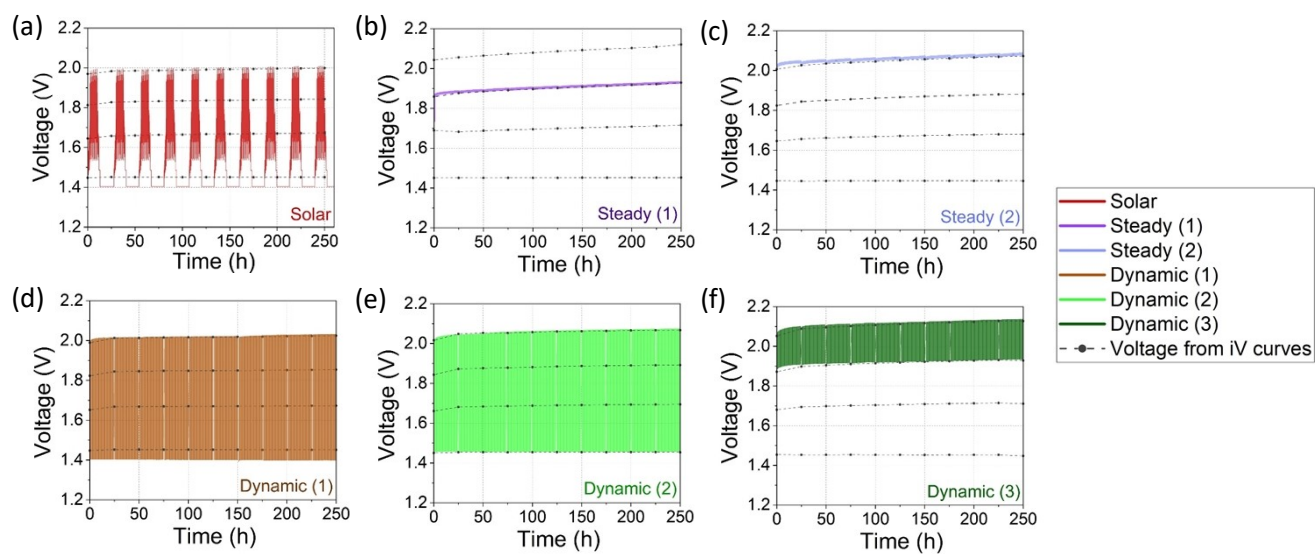
A. Main Supplementary Figures

Fig. S1: Resulted voltage profiles. (a) Solar. (b) Steady (1). (c) Steady (2). (d) Dynamic (1) profile. (e) Dynamic (2) profile. (f) Dynamic (3) profile. ⎯•⎯ represents voltage from polarization curves at 0.1, 1, 2 and 3 A cm^{-2}, that was used for the degradation rate calculation.
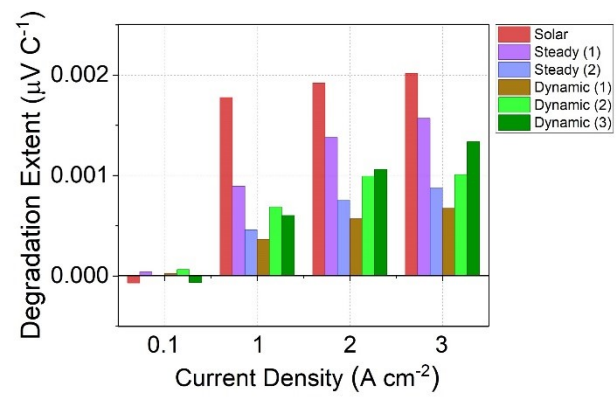
Fig. S2: Degradation extent over the charge passed.
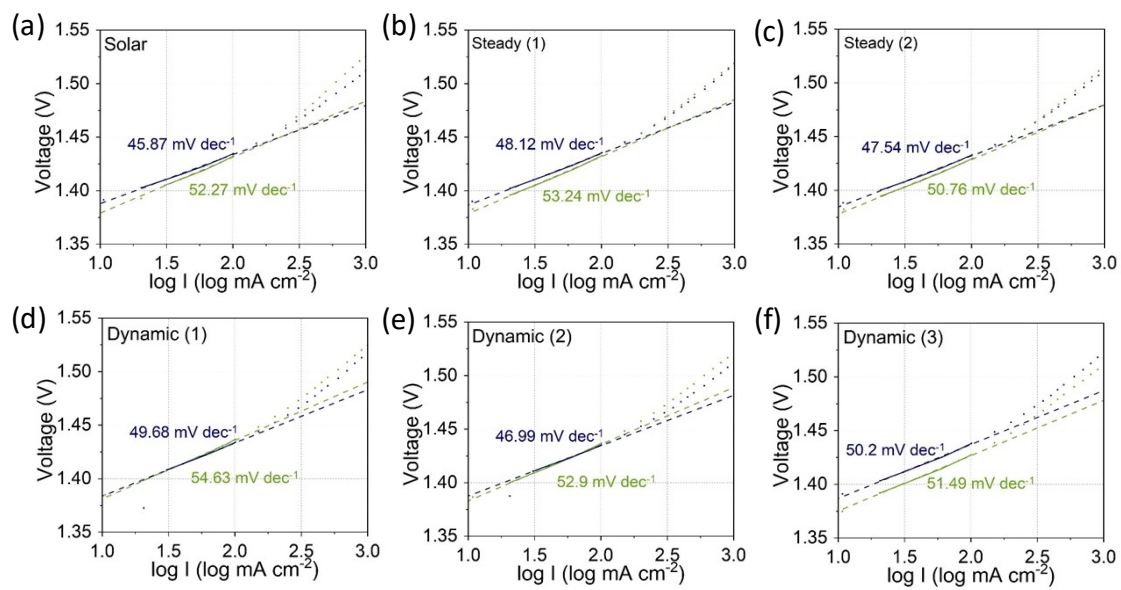
Fig. S3: Tafel slopes. (a) Solar. (b) Steady (1). (c) Steady (2). (d) Dynamic (1) load. (e) Dynamic (2) load. (f) Dynamic (3) load.
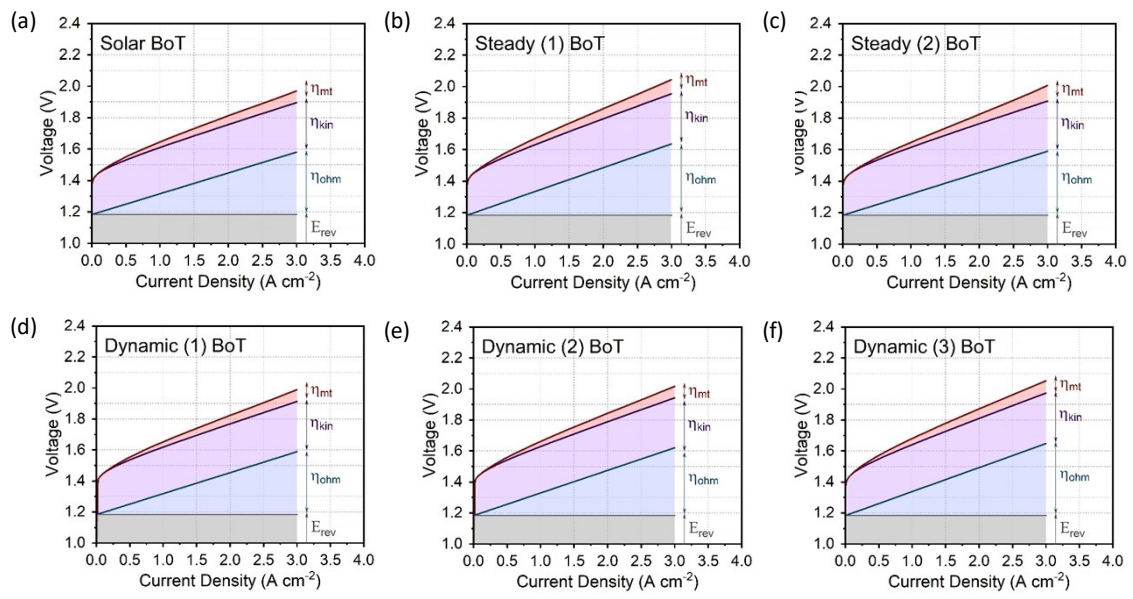
Fig. S4: BoT polarization curves breakdown. (a) Solar. (b) Steady (1). (c) Steady (2). (d) Dynamic (1). (e) Dynamic (2). (f) Dynamic (3).
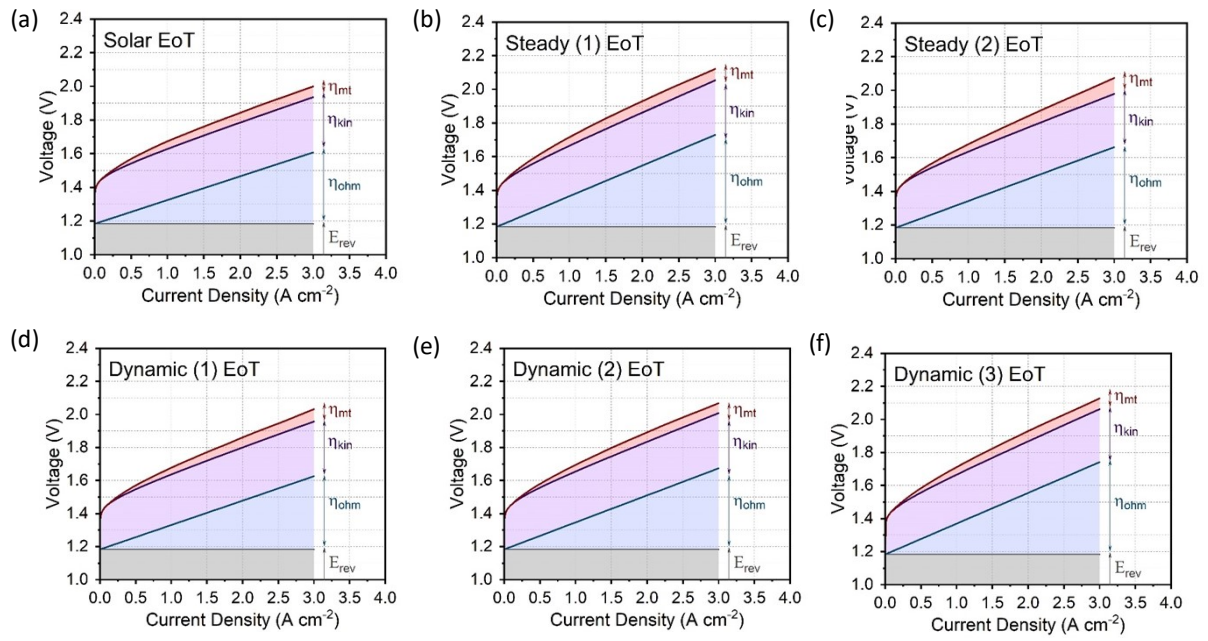
Fig. S5: EoT polarization curves breakdown. (a) Solar. (b) Steady (1). (c) Steady (2). (d) Dynamic (1). (e) Dynamic (2). (f) Dynamic (3).
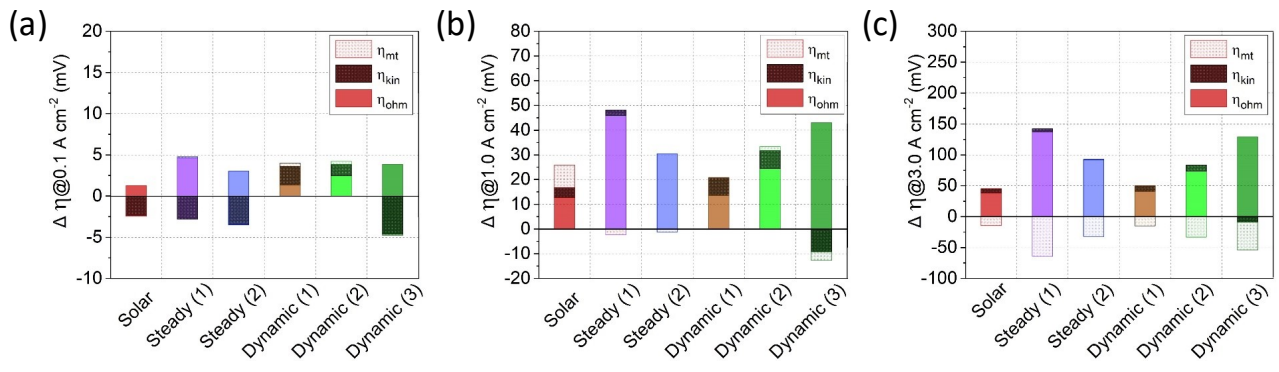
Fig. S6: Overpotential changes. (a) at 0.1 A cm^{-2}. (b) at 1 A cm^{-2}. and (c) at 3 A cm^{-2}.
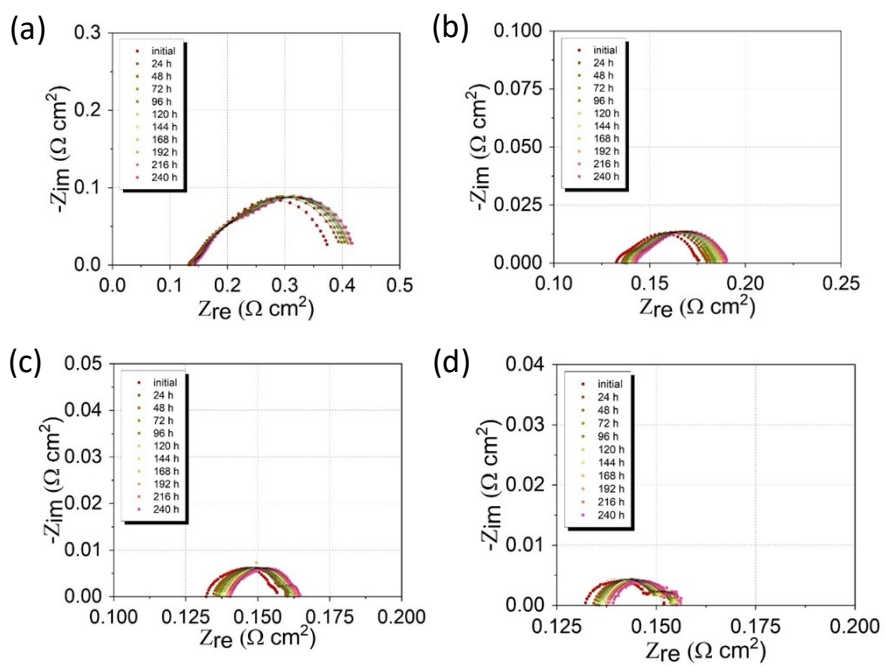
Fig. S7: Nyquist plots, obtained for Solar profile. (a) GEIS@0.1 A cm^{-2}. (b) @1 A cm^{-2}. (c) @2 A cm^{-2}. (d) @3 A cm^{-2}.
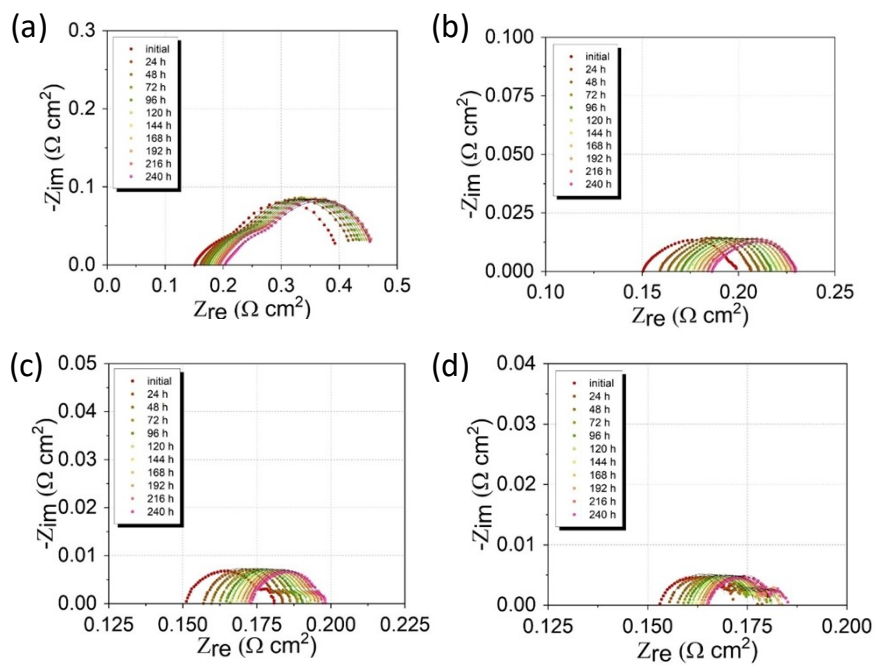
Fig. S8: Nyquist plots, obtained for Steady (1) profile. (a) GEIS@0.1 A cm^{-2}. (b) @1 A cm^{-2}. (c) @2 A cm^{-2}. (d) @3 A cm^{-2}.
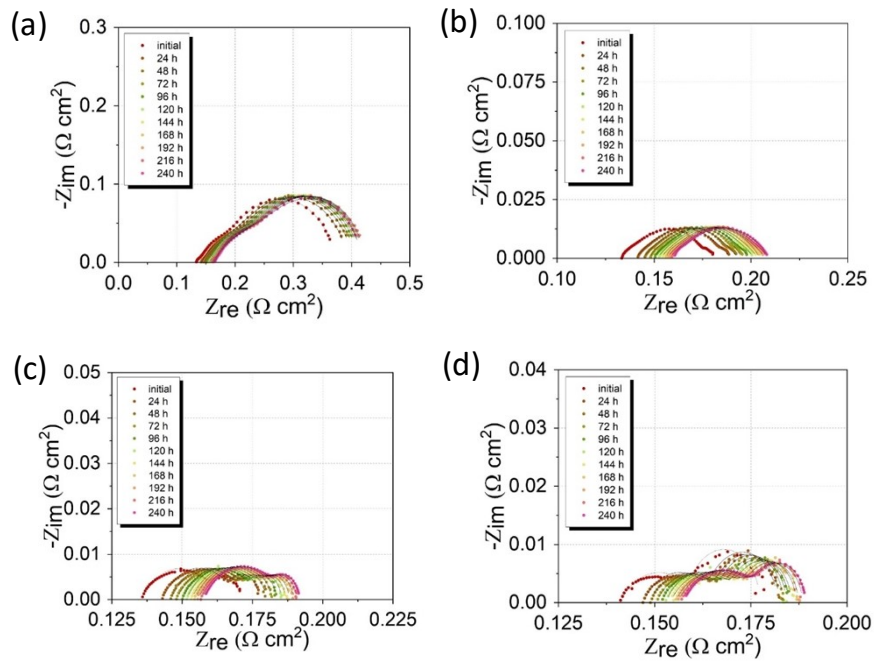
Fig. S9: Nyquist plots, obtained for Steady (2) profile. (a) GEIS@0.1 A cm^{-2}. (b) @1 A cm^{-2}. (c) @2 A cm^{-2}. (d) @3 A cm^{-2}.
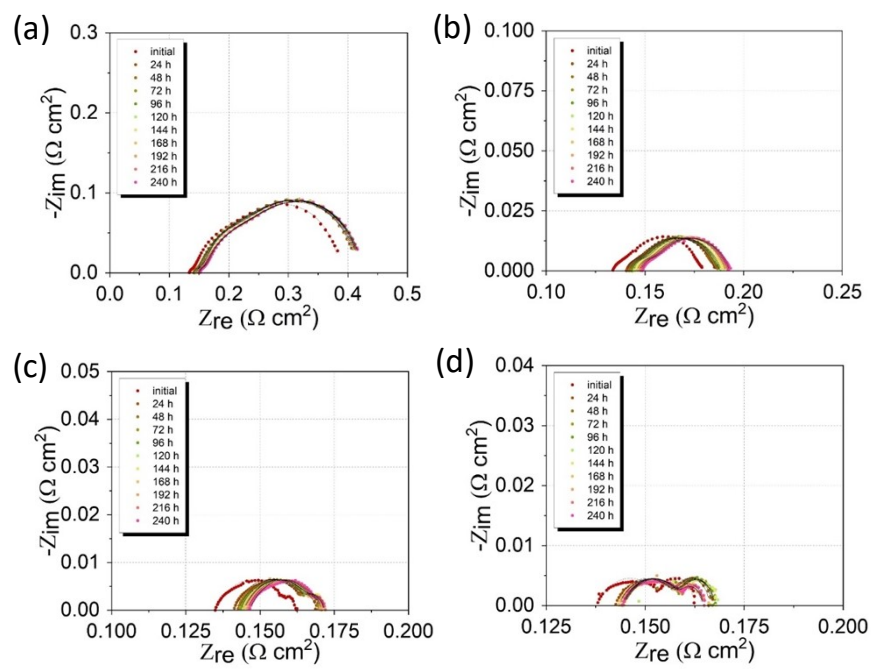
Fig. S10: Nyquist plots, obtained for Dynamic (1) profile. (a) GEIS@0.1 A cm^{-2}. (b) @1 A cm^{-2}. (c) @2 A cm^{-2}. (d) @3 A cm^{-2}.
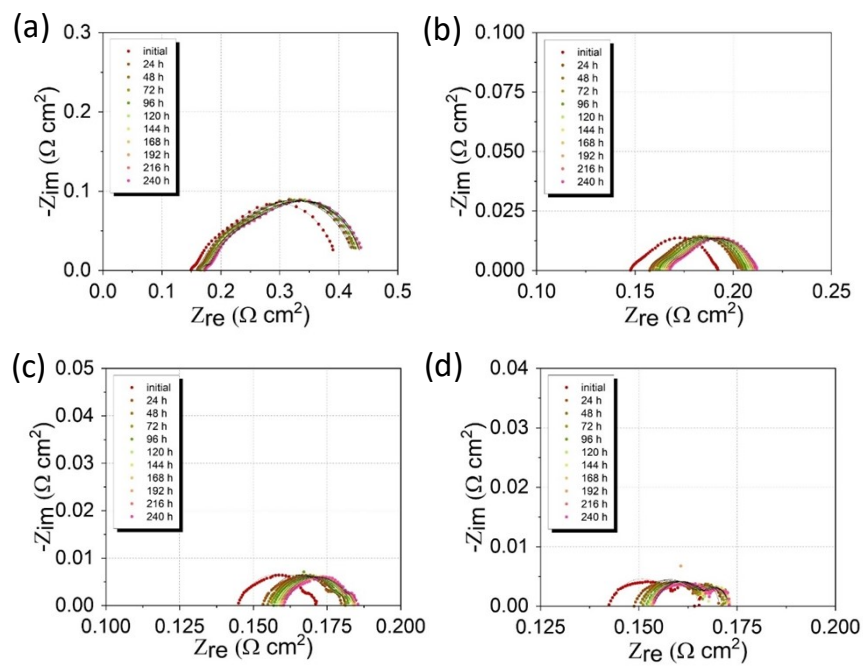
Fig. S11: Nyquist plots, obtained for Dynamic (2) profile. (a) GEIS@0.1 A cm^{-2}. (b) @1 A cm^{-2}. (c) @2 A cm^{-2}. (d) @3 A cm^{-2}.
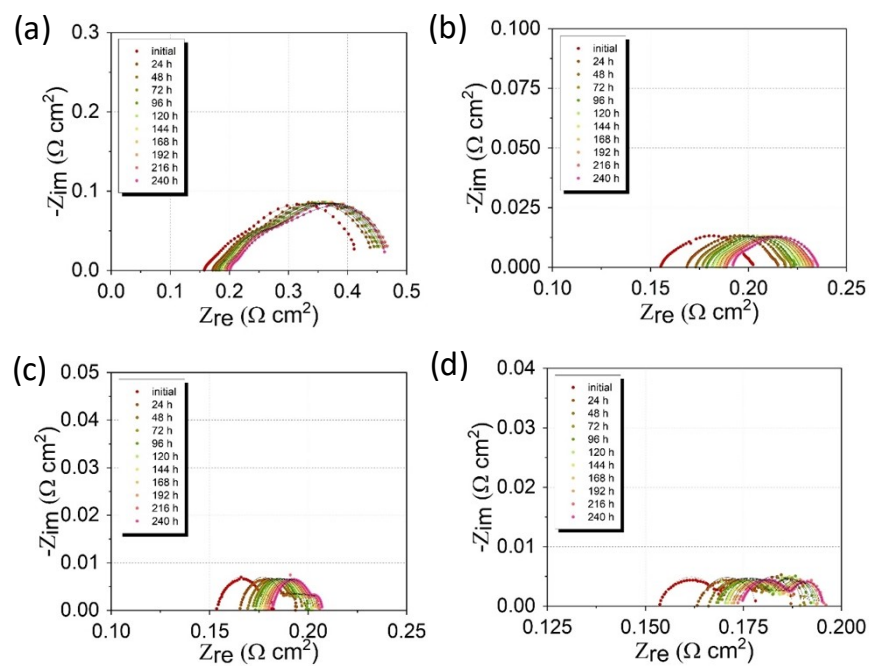
Fig. S12: Nyquist plots, obtained during Dynamic (3) profile (a) GEIS@0.1 A cm^{-2}. (b) @1 A cm^{-2}. (c) @2 A cm^{-2}. (d) @3 A cm^{-2}.
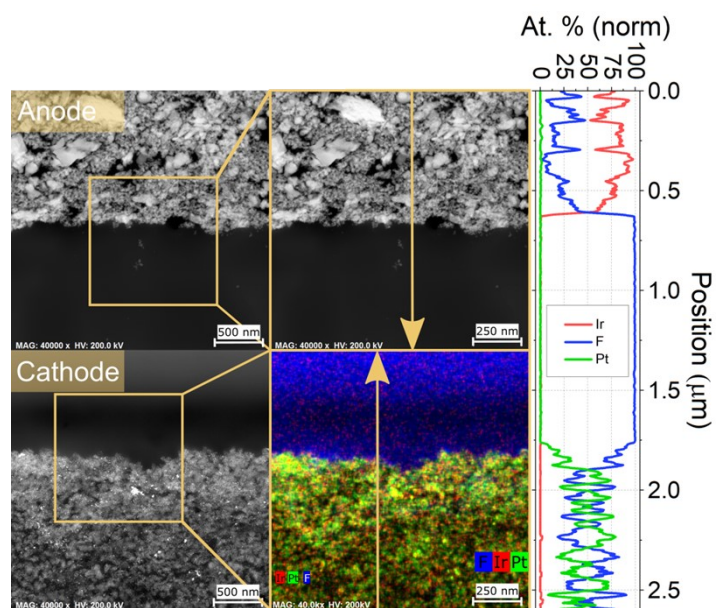
Fig. S13: Catalyst/membrane interface cross-section TEM images and EDS mapping for BoT sample.

Fig. S14: Catalyst/membrane interface analysis of the sample after Solar profile. (a) Anode/membrane interface TEM image. (b) Anode/membrane interface HAADF image. (c) Anode/membrane interface EDS mapping. (d) Anode/membrane interface TEM image of zoomed area. (e) Cathode/membrane interface TEM image. (f) Cathode/membrane interface HAADF image. (g) Cathode/membrane interface EDS mapping. (h) Anode/membrane interface TEM image of zoomed area. (Corresponding **Table S2**)

Fig. S15: Catalyst/membrane interface analysis of the sample after Steady (1) profile. (a) Anode/membrane interface TEM image. (b) Anode/membrane interface HAADF image. (c) Anode/membrane interface EDS mapping. (d) Cathode/membrane interface TEM image. (e) Cathode/membrane interface HAADF image. (f) Cathode/membrane interface EDS mapping. (Corresponding **Table S3**)
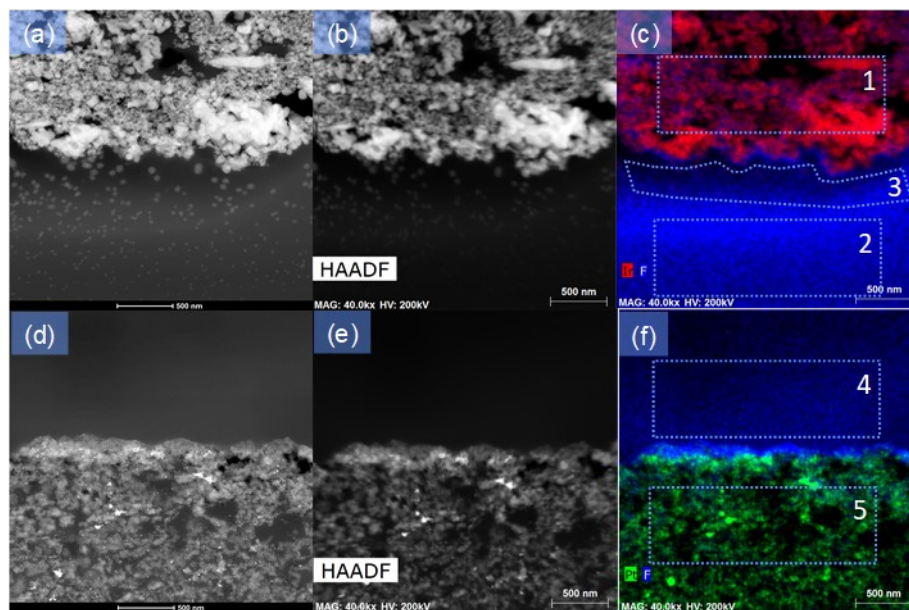
Fig. S16: Catalyst/membrane interface analysis of the sample after Steady (2) profile. (a) Anode/membrane interface TEM image. (b) Anode/membrane interface HAADF image. (c) Anode/membrane interface EDS mapping. (d) Cathode/membrane interface TEM image. (e) Cathode/membrane interface HAADF image. (f) Cathode/membrane interface EDS mapping. (Corresponding **Table S4**)
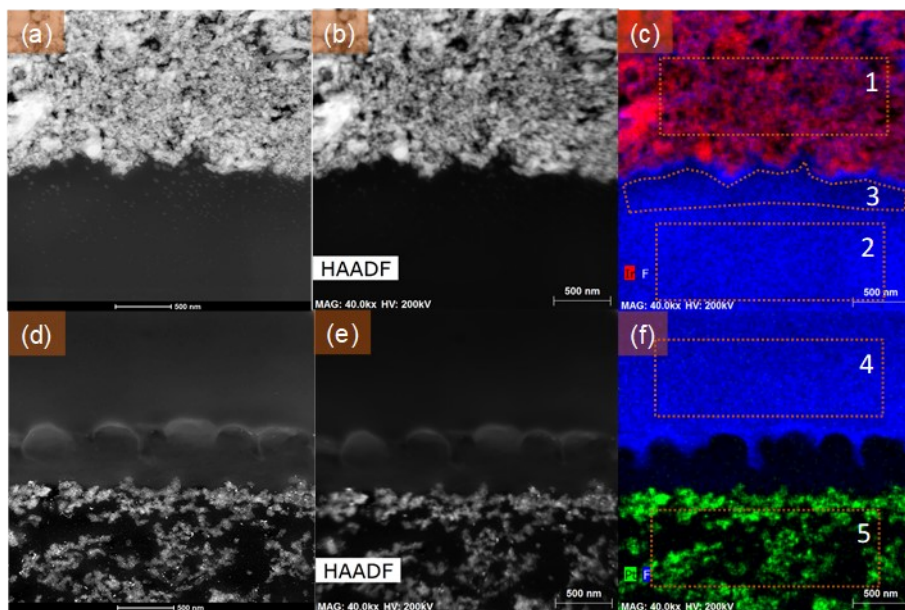
Fig. S17. Catalyst/membrane interface analysis of the sample after Dynamic (1) profile. (a) Anode/membrane interface TEM image. (b) Anode/membrane interface HAADF image. (c) Anode/membrane interface EDS mapping. (d) Cathode/membrane interface TEM image. (e) Cathode/membrane interface HAADF image. (f) Cathode/membrane interface EDS mapping. (Corresponding **Table S5**)
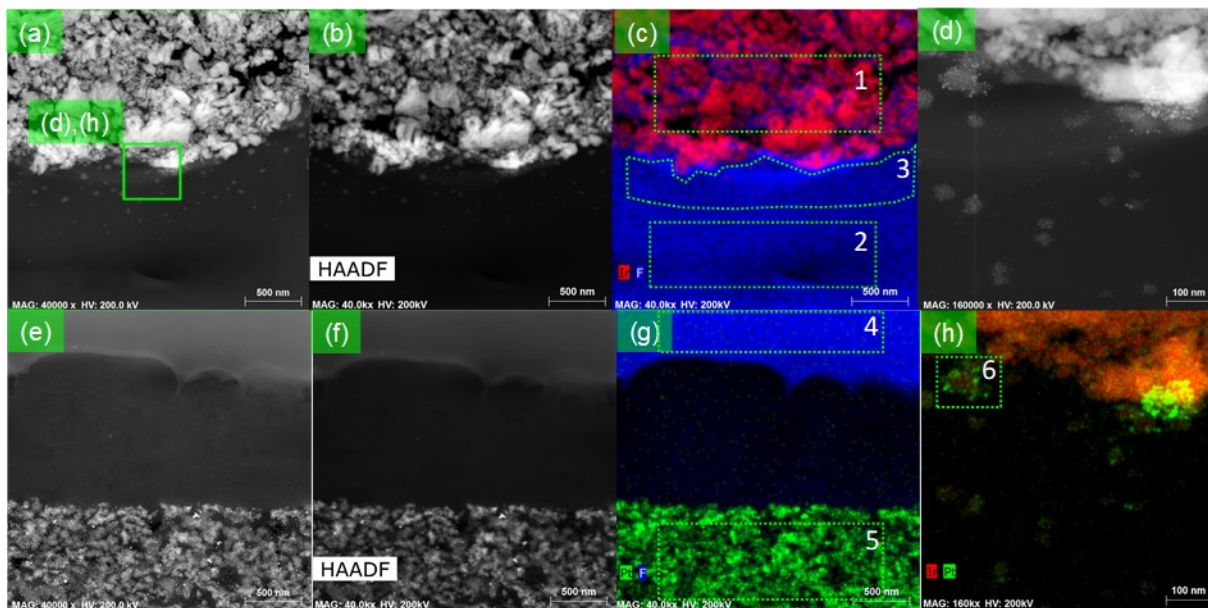
Fig. S18: Catalyst/membrane interface analysis of the sample after Dynamic (2) profile. (a) Anode/membrane interface TEM image. (b) Anode/membrane interface HAADF image. (c) Anode/membrane interface EDS mapping. (d) Anode/membrane interface TEM image of zoomed area. (e) Cathode/membrane interface TEM image. (f) Cathode/membrane interface HAADF image. (g) Cathode/membrane interface EDS mapping. (h) Anode/membrane interface TEM image of zoomed area. (Corresponding **Table S6**)
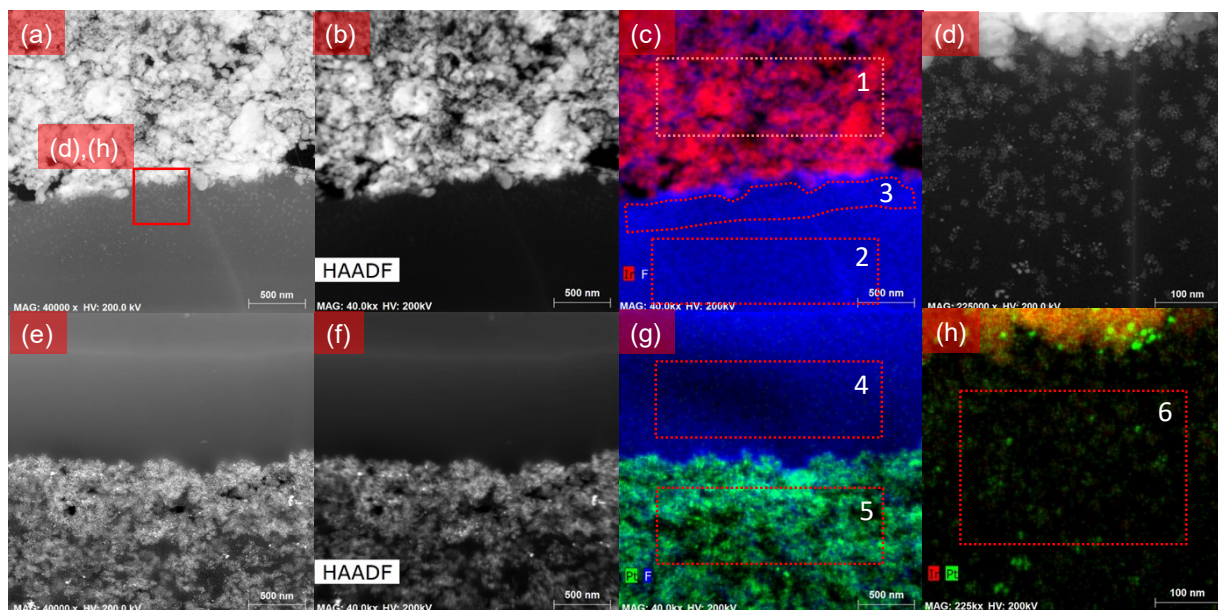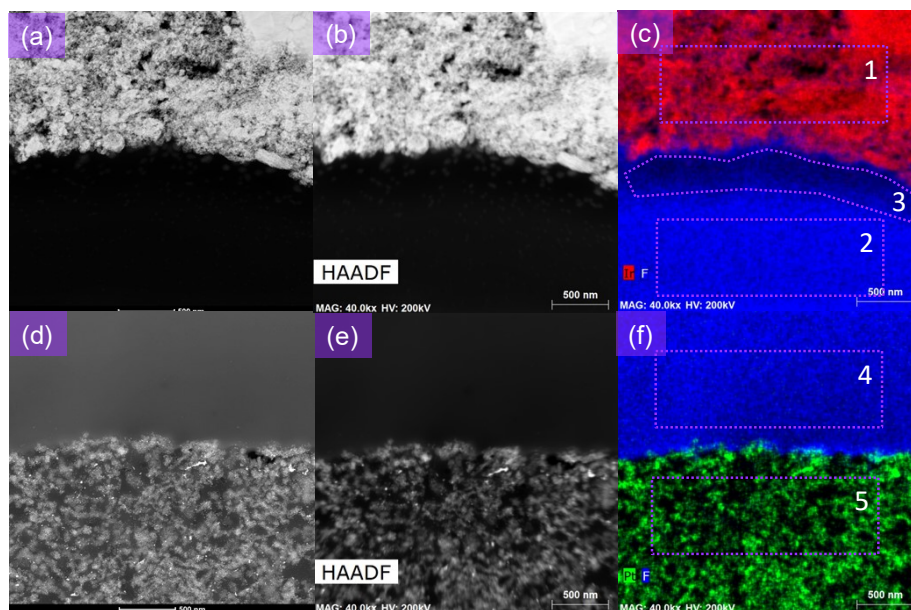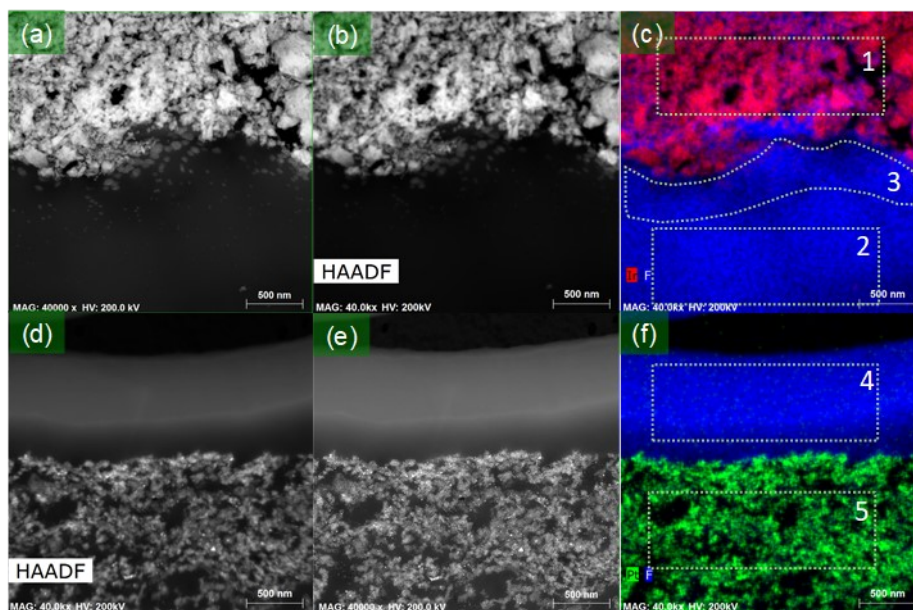
Fig. S19: Catalyst/membrane interface analysis of the sample after Dynamic (3) profile. (a) Anode/membrane interface TEM image. (b) Anode/membrane interface HAADF image. (c) Anode/membrane interface EDS mapping. (d) Cathode/membrane interface TEM image. (e) Cathode/membrane interface HAADF image. (f) Cathode/membrane interface EDS mapping. (Corresponding **Table S7**)

Table S1. Quantification results of the BoT sample

Area	E, atom C (at%)		
	Ir	Pt	F
1	82.39	1.38	16.23
2	0.05	0.00	99.95
3	0.00	0.01	99.99
4	0.51	54.77	44.72

Table S2. Quantification results of the Solar sample

Area	E, atom C (at%)		
	Ir	Pt	F
1	74.39	2.26	23.34
2	0.05	0.04	99.90
3	0.69	0.17	99.14
4	0.00	0.00	100.00
5	0.19	24.16	75.65
6	1.10	0.37	98.57

Table S3. Quantification results of the Steady (1) sample

Area	E, atom C (at%)		
	Ir	Pt	F
1	82.20	1.16	16.65
2	0.07	0.00	99.93
3	0.94	0.00	99.06
4	0.00	0.01	99.99
5	0.34	56.22	43.43

Table S4. Quantification results of the Steady (2) sample

Area	E, atom C (at%)		
	Ir	Pt	F
1	66.01	0.89	33.10
2	0.23	0.01	99.75
3	1.33	0.03	98.65
4	0.00	0.00	100.00
5	0.41	34.08	65.50

Table S5. Quantification results of the Dynamic (1) sample

Area	E, atom C (at%)		
	Ir	Pt	F
1	65.96	1.24	32.80
2	0.04	0.00	99.96
3	0.34	0.01	99.65
4	0.00	0.00	100.00
5	0.33	69.88	29.79

Table S6. Quantification results of the Dynamic (2) sample

Area	E, atom C (at%)		
	Ir	Pt	F
1	79.00	0.99	20.01
2	0.02	0.01	99.97
3	0.79	0.20	99.02
4	0.00	0.00	100.00
5	0.16	53.58	46.26
6	7.71	3.84	88.45

Table S7. Quantification results of the Dynamic (3) sample

Area	E, atom C (at%)		
	Ir	Pt	F
1	81.39	1.09	17.52
2	0.05	0.00	99.95
3	1.34	0.00	98.66
4	0.00	0.00	100.00
5	5.43	43.35	51.22
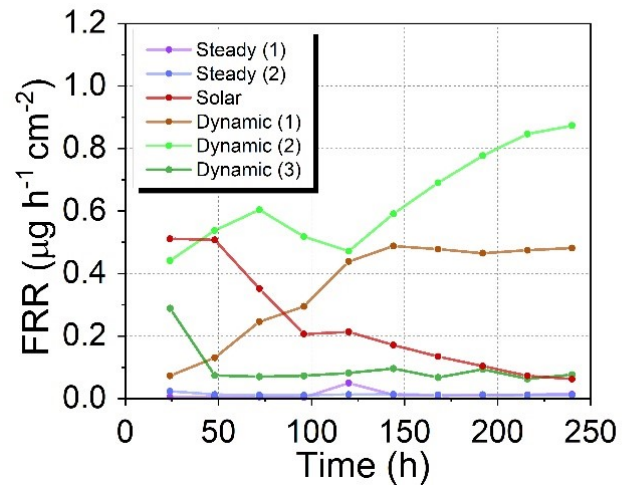
Fig. S20. FRR dynamics over time

Table S8. Nafion degradation features

Nafion degradation features		
Sample designation	FR240 (μg cm^{-2})	Membrane thickness (μm)
BoT	-	174.38±14.94
Solar	49.17	148.01±10.92
Steady (1)	2.81	178.67±21.06
Steady (2)	2.76	160.24±17.15
Dynamic (1)	79.01	143.65±7.14
Dynamic (2)	136.65	134.05±21.04
Dynamic (3)	19.24	156.46±5.69
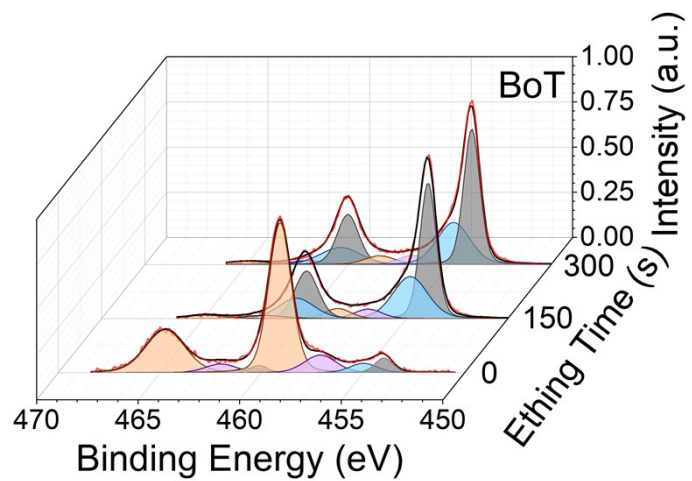
Fig. S21: Pristine Ti porous transport layer passivation. Curve-fitted X-ray photoelectron spectra attributed to the 0, 150, and 300 s of etching.

Table S9. Ti 2p$_{3/2}$ literature values from the http://www.xpsfitting.com/

Compound	Ti 2p$_{3/2}$ Peak position (eV)	Std. Dev. (eV)	Spin-orbit splitting (eV)	Std. Dev. (eV)
Ti (0)	453.9	0.3	6.1	0.06
Ti (II) oxide	455.5	0.6	5.6	-
Ti (III) oxide	457.3	0.7	5.2	-
Ti (IV) oxide	458.7	0.2	5.7	0.08

Table S10. Ti 2p$_{3/2}$ and Ti 2p$_{1/2}$ peak position and area, derived from the XPS fitting.

Sample	Etching time (s)	Ti 2p$_{3/2}$							
		Ti(0)		Ti(II)		Ti(III)		Ti(IV)	
		Peak position (eV)	Area	Peak position (eV)	Area	Peak position (eV)	Area	Peak position (eV)	Area
BoT	0	453.97	0.1	454.97	0.1	457.1	0.212	459.08	1.273
	150	453.92	0.837	454.8	0.549	456.87	0.1	458.55	0.1
	300	453.9	0.822	454.8	0.521	456.82	0.1	458.43	0.1
Solar	0	453.8	0.05	456.18	0.05	457.5	0.1	459.12	1.05
	50	453.86	0.821	454.8	0.392	456.6	0.1	458.43	0.1
	100	453.85	0.846	454.8	0.339	456.6	0.1	458.52	0.1
Steady (1)	0	453.8	0.05	455.6	0.05	457.3	0.1	459.08	1.04
	150	454.18	0.115	455.39	0.668	457.1	0.974	458.96	1.231
	300	454.17	0.735	455.2	0.963	457.1	0.74	458.92	0.728
Steady (2)	0	453.8	0.05	455.56	0.05	457.8	0.1	459.14	1.075
	150	454.18	0.141	455.43	0.698	457.28	0.853	459.06	1.117
	300	454.13	0.804	455.19	0.807	457.1	0.691	458.95	0.595
Dynamic (1)	0	453.82	0.054	455.6	0.021	457.9	0.109	459.1	1.281
	150	454.18	0.17	455.53	0.688	457.57	0.776	459.17	1.061
	300	454.11	0.684	455.18	0.698	457.1	0.837	459.12	1.051
Dynamic (2)	0	453.65	0.05	455.6	0.02	457.85	0.103	458.74	1.174
	150	453.89	0.806	454.8	0.684	457.1	0.1	458.58	0.1
	300	453.88	0.862	454.8	0.474	456.6	0.1	458.5	0.1
Dynamic (3)	0	453.65	0.051	455.6	0.02	457.9	0.1	459.1	1.098
	150	453.9	0.848	454.8	0.399	456.6	0.1	458.5	0.1
	300	453.908	0.808	454.8	0.483	456.7	0.067	458.5	0.07

Sample	Etching time (s)	Ti 2p$_{1/2}$							
		Ti(0)		Ti(II)		Ti(III)		Ti(IV)	
		Peak position (eV)	Area	Peak position (eV)	Area	Peak position (eV)	Area	Peak position (eV)	Area
BoT	0	460.12	0.05	460.56	0.05	462	0.106	464.73	0.636
	150	459.91	0.419	460.51	0.274	462	0.05	464.9	0.05
	300	460	0.411	460.55	0.261	462	0.05	464.9	0.05
Solar	0	460	0.025	460.9	0.025	462.18	0.05	464.78	0.527
	150	459.91	0.41	460.56	0.196	462	0.05	464.9	0.05
	300	459.91	0.423	460.69	0.169	462	0.05	464.9	0.05
Steady (1)	0	460	0.025	460.9	0.025	462.18	0.04	464.7	0.52
	150	460	0.058	460.8	0.334	462.18	0.487	464.63	0.616
	300	460.1	0.368	460.86	0.482	462.18	0.37	464.7	0.364
Steady (2)	0	460	0.025	460.9	0.025	462.5	0.05	464.88	0.537
	150	460	0.07	460.9	0.349	462.43	0.427	464.72	0.474
	300	460	0.402	460.84	0.404	462.18	0.345	464.7	0.297
Dynamic (1)	0	460.1	0.027	461.1	0.01	462.35	0.055	464.79	0.641
	150	460	0.085	460.8	0.344	462.45	0.388	464.82	0.531
	300	460	0.342	460.9	0.349	462.18	0.418	464.9	0.525
Dynamic (2)	0	460.1	0.025	460.56	0.01	462	0.052	464.46	0.587
	150	460	0.403	460.5	0.342	462.02	0.05	464.7	0.05
	300	459.91	0.431	460.6	0.237	462	0.05	464.3	0.05
Dynamic (3)	0	460.1	0.026	461.1	0.01	462.5	0.05	464.79	0.549
	150	460	0.424	460.54	0.2	462	0.05	464.3	0.05
	300	460	0.404	460.58	0.241	462	0.033	464.3	0.035
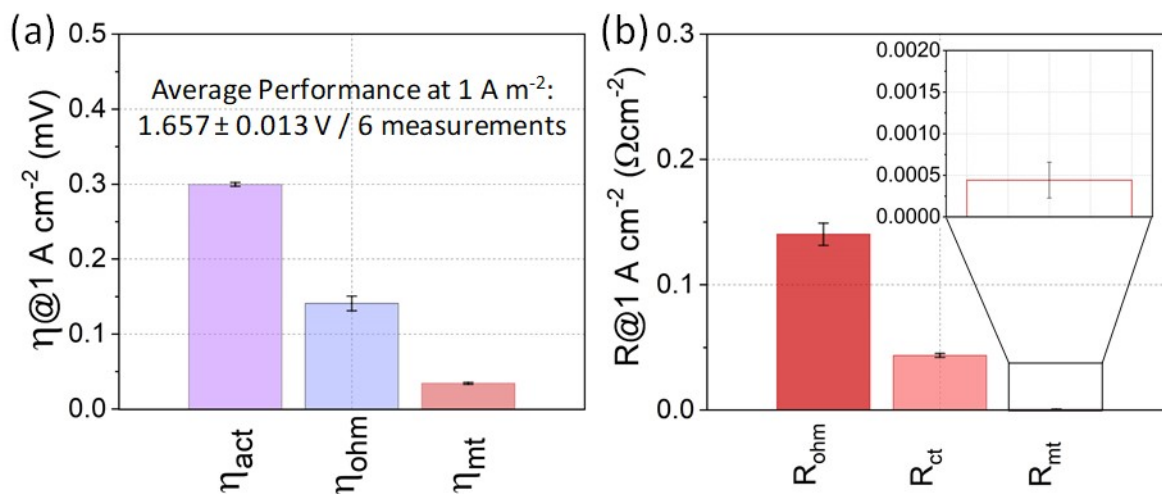
Figure S22: Reproducibility of BoT Performance. (a) Overpotentials averaged between six beginning of the test (BoT) measurements for each profile with the standard deviation. (b) R_{ohm}, R_{ct}, and R_{mt} averaged between six BoT measurements for each profile with the standard deviation. Overpotentials were calculated from the polarization curves decoupling, and R_{ohm}, R_{ct}, and R_{mt} were calculated from the Nyquist plot z-fit analysis.
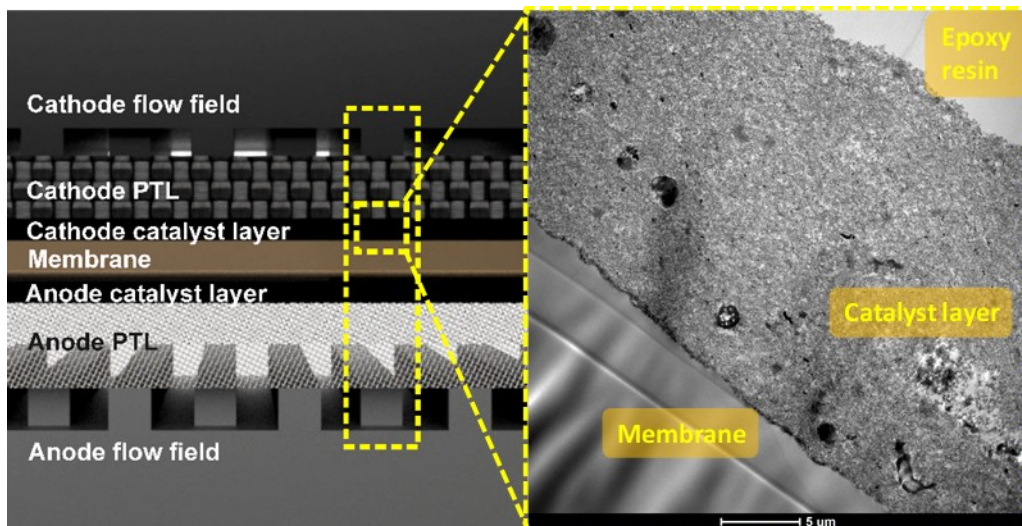
Fig. S23: Microtome sampling and slice TEM image example.

B. Cell operating conditions optimization

Cell conditioning
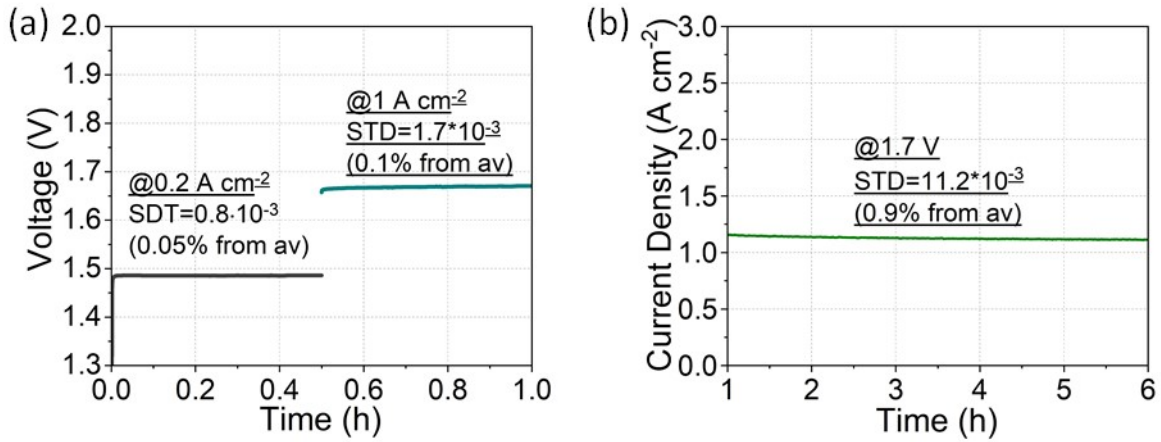
Fig. S_B1: Cell conditioning profiles. Conditioning protocol is adapted from [1]

Cell conditioning protocol, adapted from[1], consisted from the chronopotentiometry at 0.2 A cm^{-2} during 0.5 h, followed by the chronopotentiometry at 1 A cm^{-2} during 0.5 h and chronoamperometry at 1.7 V till the current variations will be lower than 1 % (applied duration was 5 h). Samples remained stable during conditioning step, voltage and current profiles examples for one sample can be seen in **Fig. S_B1**.

Cell clamping force optimization

The clamping force F_c was calculated, using the following equation (1) [2]:

$$F_c = \frac{T \cdot N}{f \cdot D} \tag{1}$$

where T is the applied on each bolt torque (N m); N is the number of bolts; f is the friction coefficient (0.2 for steel bolts); D is the nominal bolt diameter (m).
The applied clamping pressure P_c was calculated, as a function of the clamping force F_c (N) and contact area A_c (m^2) in accordance with the equation (2):

$$P_c = \frac{F_c}{A_c} \tag{2}$$

Table S_B1. Clamping pressure calculation

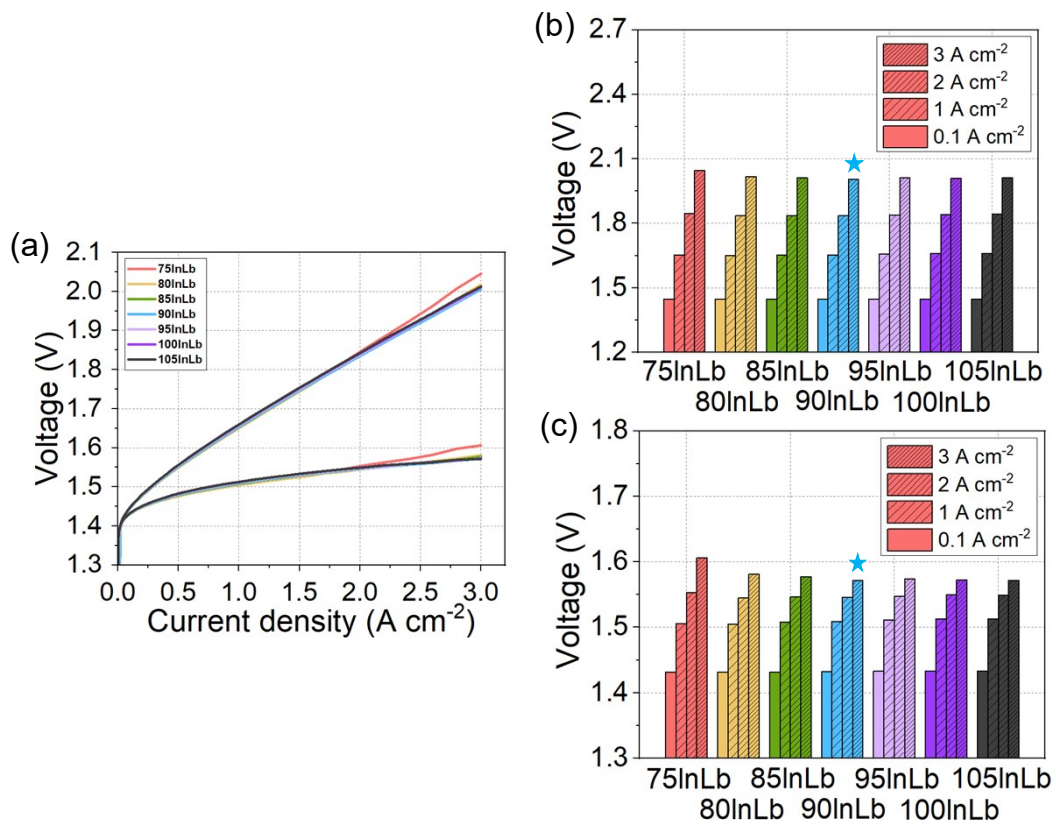| Sample designation	P_c (MPa)	F_c (N)	A_c (m²)	N (-)	T (N m)	f (-)	D (m)
75InLb	2.35	33892.00	0.0144	8	8.47	0.2	0.01
80InLb	2.51	36152.00			9.04		
85InLb	2.52	36241.20			9.06		
90InLb	2.82	40674.40			10.17		
95InLb	2.98	42934.00			10.73		
100InLb	3.14	45193.60			11.30		
105InLb	3.30	47453.60			11.86		

Fig. S_B2: Effect of the clamping force on the performance. (a) Polarization curves. (b) Performance comparison under specific current densities. (c) Performance comparison under specific current densities, subtracted from the iR-corrected polarization curves. Optimal clamping pressure is marked with ★.

Table S_B2. Cell performance comparison under different applied clamping forces

Sample designation	Performance @0.1 A cm^{-2} (V)		Performance @1 A cm^{-2} (V)		Performance @2 A cm^{-2} (V)		Performance @3 A cm^{-2} (V)	
	Non-corr.	iR-corr.	Non-corr.	iR-corr.	Non-corr.	iR-corr.	Non-corr.	iR-corr.
75InLb	1.4463	1.4315	1.6518	1.5053	1.8459	1.5530	2.0455	1.6063
80InLb	1.4464	1.4317	1.6503	1.5046	1.8363	1.5450	2.0178	1.5808
85InLb	1.4463	1.4316	1.6526	1.5077	1.8359	1.5463	2.0117	1.5773
90InLb	1.4468	1.4322	1.6534	1.5089	1.8348	1.5459	2.0051	1.5718
95InLb	1.4479	1.4332	1.6568	1.5110	1.8388	1.5473	2.0107	1.5735
100InLb	1.4481	1.4334	1.6590	1.5129	1.8416	1.5495	2.0105	1.5726
105InLb	1.4481	1.4333	1.6594	1.5124	1.8426	1.5489	2.0123	1.5718
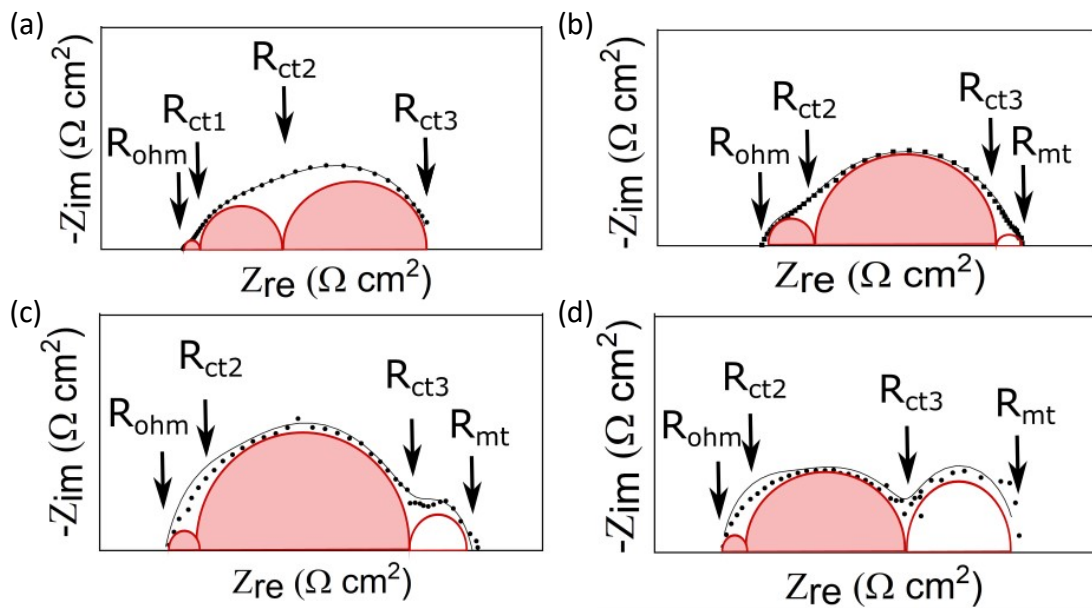
Fig. S_B3: Schematic description for the resistance evaluation. (a) GEIS@0.1 A cm^{-2}. (b) @1 A cm^{-2}. (c) @2 A cm^{-2}. (d) @3 A cm^{-2}. R_{ohm} corresponds to ohmic resistance, R_{ct1}, R_{ct2}, and R_{ct3} to charge-transfer resistances, and R_{mt} to mass transport resistance. Z-fit analysis was made using the EC-Lab software.

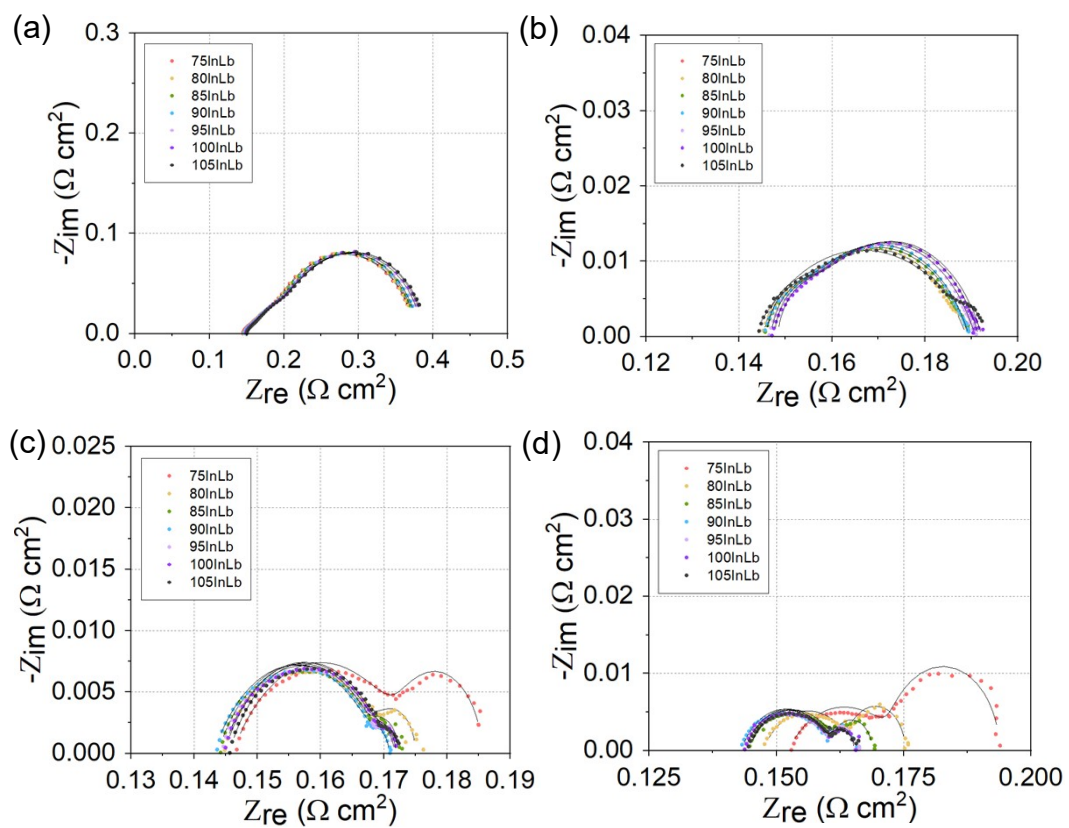**Fig. S_B4**: **Effect of the clamping force on the cell resistances.** (a) GEIS@0.1 A cm^{-2}. (b) @1 A cm^{-2}. (c) @2 A cm^{-2}. (d) @3 A cm^{-2}. Z-fit analysis was made using the EC-Lab software.

Table S_B3. Cell resistances comparison under different applied clamping force

Sample designation	Resistance @0.1 A cm^{-2} (Ω)			Resistance @1 A cm^{-2} (Ω)			Resistance @2 A cm^{-2} (Ω)			Resistance @3 A cm^{-2} (Ω)		
	R_{ohm}	R_{ct2}	R_{ct3}	R_{ohm}	R_{ct2}	R_{ct3}	R_{ohm}	R_{ct2}	R_{ct3}	R_{ohm}	R_{ct2}	R_{ct3}
75InLb	0.143	0.059	0.172	0.143	0.003	0.047	0.146	0.027	0.012	0.152	0.021	0.020
80InLb	0.145	0.062	0.168	0.145	0.005	0.038	0.144	0.025	0.005	0.147	0.017	0.010
85InLb	0.145	0.072	0.160	0.145	0.005	0.037	0.143	0.025	0.003	0.144	0.017	0.006
90InLb	0.145	0.085	0.151	0.145	0.006	0.037	0.143	0.026	0.001	0.143	0.016	0.005
95InLb	0.147	0.080	0.158	0.146	0.006	0.037	0.144	0.024	0.002	0.143	0.016	0.005
100InLb	0.147	0.092	0.150	0.147	0.006	0.037	0.144	0.025	0.002	0.143	0.016	0.004
105InLb	0.149	0.079	0.163	0.148	0.006	0.037	0.145	0.024	0.002	0.144	0.016	0.004

Water flow rate optimization

A minimum amount of water supply, which is needed for the electrochemical reaction can be calculated from the Faraday's Law, taking into account the operation current density. Thus, the molar rate of water consumption for the anode reaction can be calculated in accordance with the equation (3):

$$N = \frac{i \cdot A}{2 \cdot F} \qquad (3)$$

where i is the operation current density (A cm^{-2}); A is the electrode active area (cm²); F is the Faraday's constant (96485.3 C mol^{-1}). Taking into account electroosmotic drag to the cathode and additional water supply in order to prevent electrode starvation or membrane degradation, the ratio of the needed inlet water supply to the water amount, required to sustain only the electrochemical reaction, can be calculated in accordance with the equation (4) [3]:

$$\varepsilon = \frac{G_{circ}}{G_{cons} + G_{drag}} \qquad (4)$$

where G_{circ} is the mass flux of the inlet water (ml min^{-1}); G_{cons} is the mass flux of water consumed by the anode reaction (ml min^{-1}); and G_{drag} is the water transported by the electroosmotic drag to the cathode (ml min^{-1}). The optimal water flow rate was established, assuming ε as 7, 8 and 9. Corresponding calculations can be seen in **Table S_B4**.

Table S_B4. Inlet water flow rate calculation

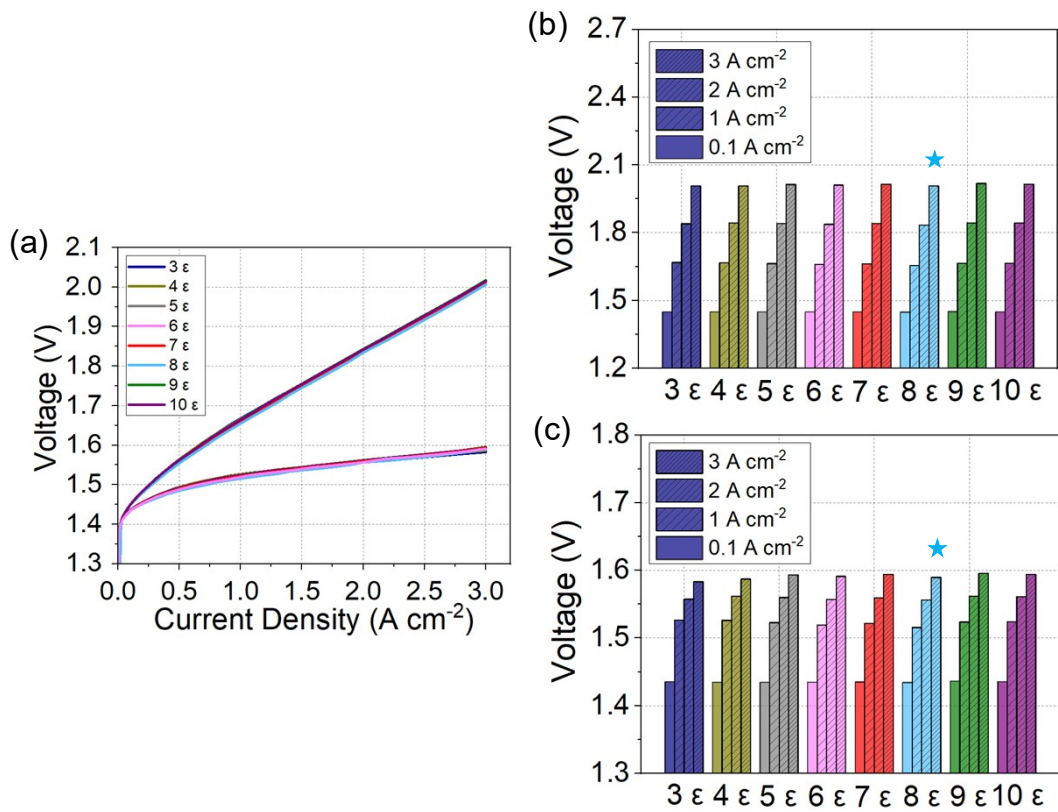| Sample designation	i (A cm^{-2})	A (cm²)	F (C mol^{-1})	ε (-)	G_{circ} (ml min^{-1})	G_{cons} (ml min^{-1})	G_{drag} (ml min^{-1})
3 ε				3	13.8		
4 ε				4	18.5		
5 ε				5	23.1		
6 ε	3	25	96485.3	6	27.7	0.41	4.19
7 ε				7	32.3		
8 ε				8	36.9		
9 ε				9	41.5		
10 ε				10	46.2		

Fig. S_B5: Effect of the water flow rate on the performance. (a) Polarization curves. (b) Performance comparison under specific current densities. (c) Performance comparison under specific current densities, subtracted from the iR-corrected polarization curves. Optimal clamping pressure is marked with ⭐.

Table S_B5. Cell performance comparison under different water flow rates

| Sample designation	Performance @0.1 A cm^{-2} (V)		Performance @1 A cm^{-2} (V)		Performance @2 A cm^{-2} (V)		Performance @3 A cm^{-2} (V)	
	Non-corr.	iR-corr.	Non-corr.	iR-corr.	Non-corr.	iR-corr.	Non-corr.	iR-corr.
3 ε	1.4495	1.4352	1.6676	1.5263	1.8396	1.5573	2.0064	1.5830
4 ε	1.4490	1.4348	1.6663	1.5260	1.8419	1.5615	2.0076	1.5870
5 ε	1.4490	1.4348	1.6627	1.5226	1.8398	1.5597	2.0132	1.5931
6 ε	1.4486	1.4344	1.6592	1.5193	1.8366	1.5570	2.0104	1.5910
7 ε	1.4491	1.4349	1.6619	1.5216	1.8399	1.5596	2.0143	1.5938
8 ε	1.4482	1.4341	1.6546	1.5155	1.8341	1.5562	2.0062	1.5894
9 ε	1.4502	1.4359	1.6644	1.5235	1.8432	1.5616	2.0175	1.5952
10 ε	1.4498	1.4356	1.6645	1.5239	1.8419	1.5610	2.0149	1.5937
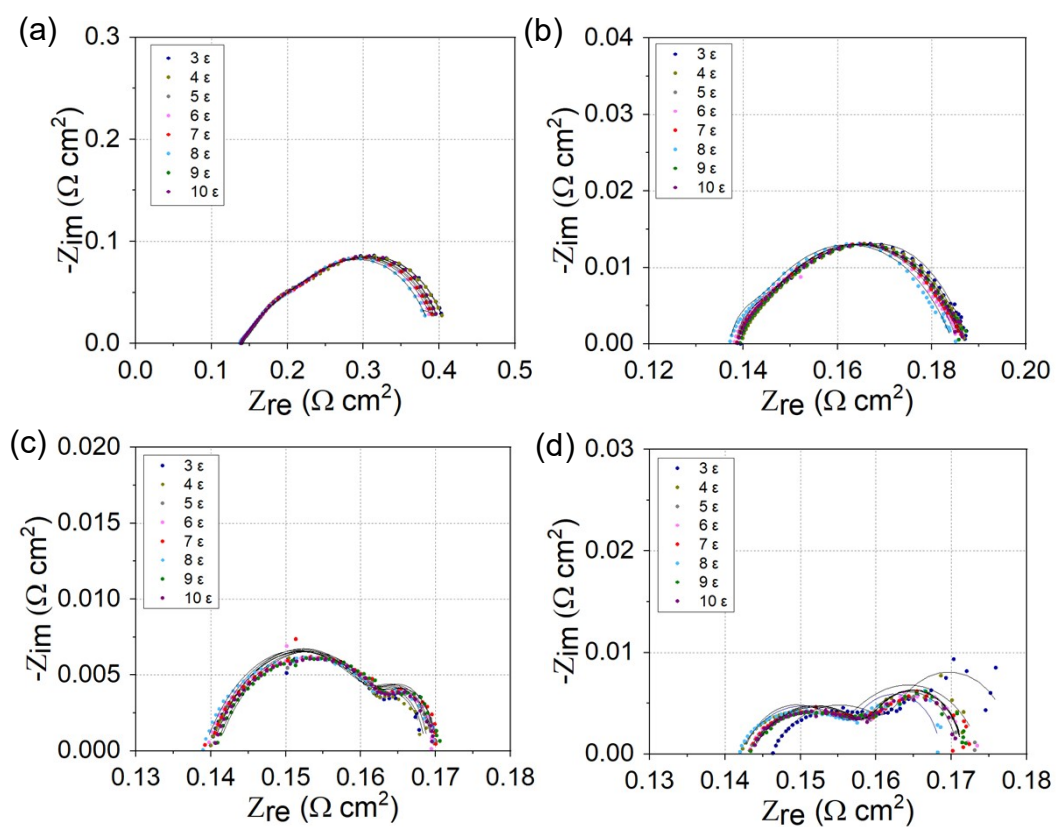
Fig. S_B6: Effect of the water flow rate on cell resistances. (a) GEIS@0.1 A cm^{-2}. (b) @1 A cm^{-2}. (c) @2 A cm^{-2}. (d) @3 A cm^{-2}. Z-fit analysis was made using the EC-Lab software.

Table S_B6. Cell resistances comparison under different applied clamping force

Sample designation	Resistance @0.1 A cm^{-2} (Ω)			Resistance @1 A cm^{-2} (Ω)			Resistance @2 A cm^{-2} (Ω)			Resistance @3 A cm^{-2} (Ω)		
	R_{ohm}	$R_{ct,c}$	$R_{ct,a}$	R_{ohm}	$R_{ct,c}$	$R_{ct,a}$	R_{ohm}	$R_{ct,c}$	$R_{ct,a}$	R_{ohm}	$R_{ct,c}$	$R_{ct,a}$
3 ε	0.139	0.114	0.162	0.138	0.007	0.041	0.139	0.025	0.007	0.146	0.017	0.014
4 ε	0.139	0.096	0.181	0.139	0.005	0.042	0.139	0.024	0.004	0.142	0.015	0.010
5 ε	0.138	0.095	0.174	0.138	0.003	0.044	0.14	0.024	0.005	0.143	0.017	0.011
6 ε	0.138	0.096	0.169	0.138	0.004	0.042	0.139	0.024	0.005	0.143	0.017	0.011
7 ε	0.138	0.097	0.170	0.138	0.003	0.044	0.14	0.024	0.006	0.143	0.016	0.011
8 ε	0.137	0.098	0.143	0.137	0.003	0.043	0.139	0.024	0.005	0.142	0.017	0.009
9 ε	0.139	0.099	0.172	0.139	0.003	0.044	0.140	0.024	0.005	0.143	0.017	0.011
10 ε	0.138	0.098	0.174	0.139	0.003	0.044	0.140	0.023	0.005	0.143	0.016	0.011

Simulation of RES - powered electrolyzer operation conditions

The implementation of a direct solar array - electrolyzer coupling (without DC/DC converter or maximum power point tracker (MPPT)) is beneficial in terms of avoiding additional losses and, as a consequence, increasing system efficiency[4]. In case of direct coupling, system operation points will be determined as the intersection points between I-V curves of the solar array and electrolyzer setup[5]. Taking into account the absence of the MPPT, the maximum power supply can be realized by selection the number of cells in solar array and cells in electrolyzer stack, that the intersection points are as close to the maximum power point (MPP) as possible[6].
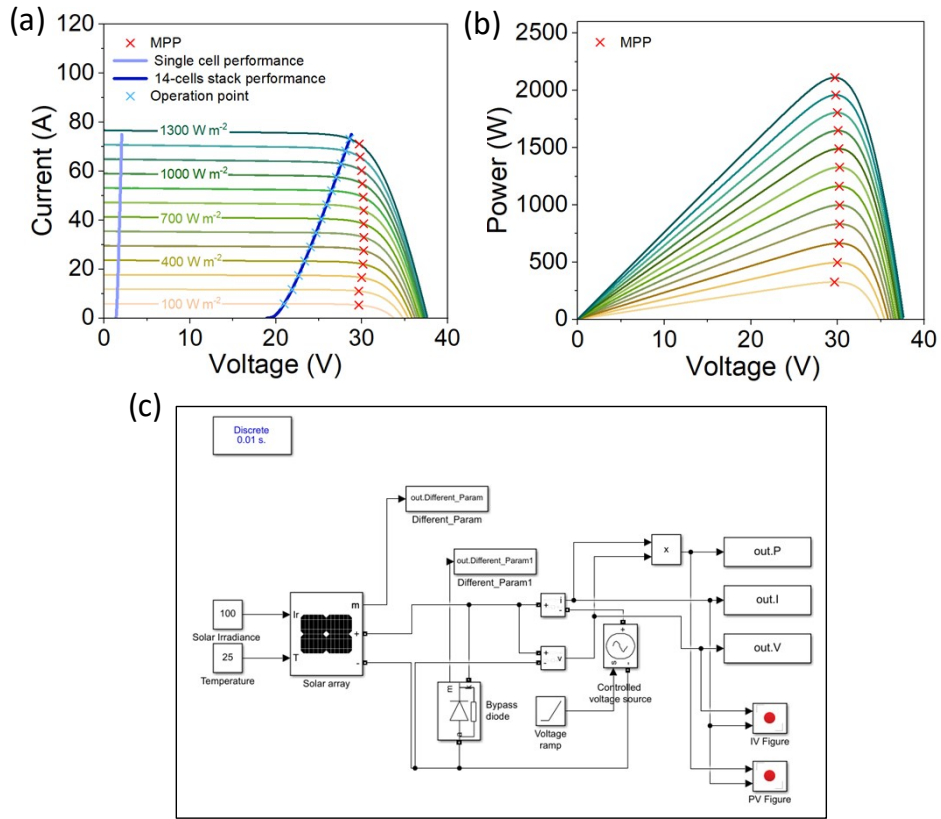

Fig. S_B7: Determination of the solar array - electrolyser direct coupling operation conditions. I-V curves of the Samsung SDI LPC235SM-02 solar array (7 parallel strings in one module, with 60 cells per module) at different irradiation levels. (a) Current–voltage characteristic of the polymer water electrolyzer single cell (measured) and stack (theoretical) are implemented. (b) P-V curves of the Samsung SDI LPC235SM-02 solar array. (c) Simulink model, created for the simulation of the I-V and P-V characteristics of the solar array.

In the current work, in order to estimate operation features of the direct coupled solar array-electrolyzer setup and compose AST protocol, that will reflect that features, first of all coupling characteristics should be assumed. I-V and P-V characteristics of the solar array were simulated. The commercially available solar array was chosen (Samsung SDI LPC235SM-02) and the number of parallel strings in the solar array was suggested in order to ensure elevated current load (3 A cm^{-2}) at 1300 W m^{-2} needed for electrolyzer operation. Theoretical I-V curves (**Fig. S_B7a**) and P-V curves (**Fig. S_B7b**) of the chosen solar array at different irradiation levels were simulated using Simulink (**Fig. S_B7c**) in accordance with the single diode model described in equation (5) [4]:

$$I = I_{ph} - I_o\left(e^{\frac{V + I \cdot R_s}{n \cdot N_s \cdot V_{th}}} - 1\right) - \frac{V + I \cdot R_s}{R_{sh}} \tag{5}$$

where I_{ph} is the photocurrent, I_o is the cell saturation current, R_s is the series resistance, n is the cell ideality factor, N_s is the number of cells in series, V_{th} is the thermal voltage and R_{sh} is the internal resistance of the cell. In turn, the photocurrent can be determined by equation (6):

$$I_{ph} = \frac{I_{sc}(R_s + R_{sh})}{R_{sh}} \tag{6}$$

where I_{sc} is the short circuit current. Also, the cell saturation current I_o can be determined by equation (7):

$$I_o = \left(\frac{I_{sc}(R_s + R_{sh}) - V_{oc}}{R_{sh}}\right) \cdot e^{-\frac{V_{oc}}{nN_sV_{th}}} \tag{7}$$

where V_{oc} is the open circuit voltage. Simulation is based on the solar cell manufacturer's technical information (**Table S_B7**), and was made assuming that temperature is constant and equal to 25 °C.

Table S_B7. Parameters of PV module Samsung SDI LPC235SM-02 at standard test conditions (T = 25 °C)[7].

Parameter description	Parameter designation	Value
Cells per module	N_s	60
Open circuit voltage	V_{oc}	37.24
Short-circuit current	I_{sc}	8.43
Cell ideality factor	n	0.98504
Shunt resistance	R_{sh}	185.6916
Series resistance	R_s	0.3551
Thermal voltage	V_{th}	0.0257 V

After simulating I-V and P-V characteristics of the chosen solar array, the number of cells in the electrolyzer stack was assumed to 14 (stack performance is theoretical and based on the practically measured performance of the single cell), in order to ensure the closest location of the operation points to the maximum power points (MPP). The obtained intersection points (operation points of the direct coupled device) made it possible to obtain a linear dependence of the input current to the solar irradiance, with the help of which highly variable solar irradiance profile[8] (**Fig. S_B8a**) was converted into an input current profile (**Fig. S_B8b**). Also should be noted, that chosen solar irradiance profile [8] has high temporal and spatial resolution and is able to track high ramp rate events, occurred due to the cloud movement [8].
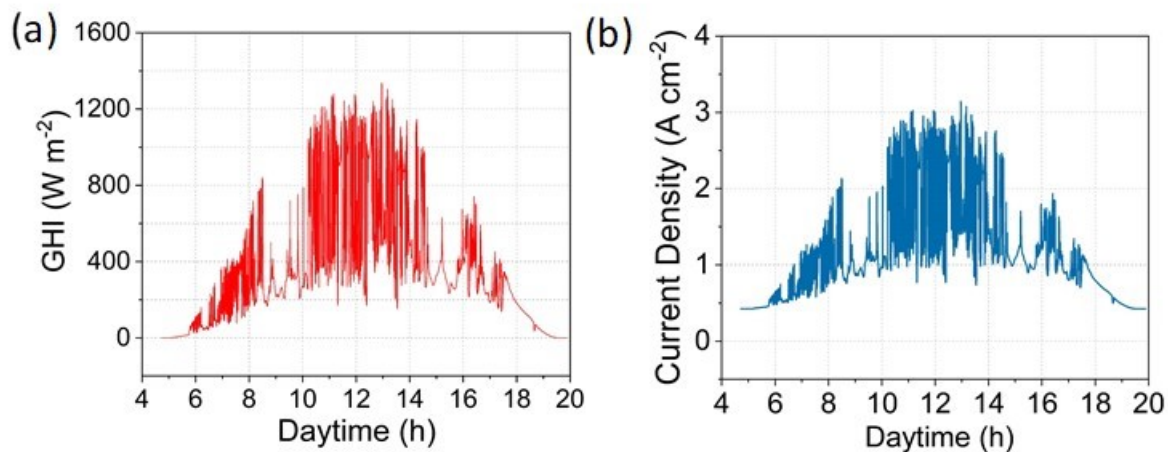

Fig. S_B8: (a) Highly variable solar irradiance profile[8]. (b) Input current profile, generated from the irradiance profile.

As the next step, the current ramp of the input current profile was estimated. In order to do that, all local maximums and minimums of the solar profile were determined, using the Python module:

```python
import numpy as np
import matplotlib.pyplot as plt
from scipy.signal import find_peaks
import pandas as pd
x1 = open("Book2.csv")
numpy_array = np.loadtxt(x1)
y1 = open("Book3.csv")
numpy_array2 = np.loadtxt(y1)
x = numpy_array
y = numpy_array2
peaks = find_peaks(y, height = 0.00001, threshold = 0.00000001, distance = 1)
height = peaks[1]['peak_heights']
peak_pos = x[peaks[0]]
y2 = y*-1
minima = find_peaks(y2)
min_pos = x[minima[0]]
min_height = y2[minima[0]]
fig = plt.Fig.()
ax = fig.subplots()
ax.plot(x,y)
ax.scatter(peak_pos, height, color = 'r', s = 15, marker = 'X', label = 'Maximum')
ax.scatter(min_pos, min_height*-1, color = 'b', s = 15, marker = 'X', label = 'Minimum')
ax.legend()
ax.grid()
plt.show()
import csv
datawindow4 = peak_pos
with open("max x.csv", "w") as f:
    for d in datawindow4:
        f.write(str(d))
        f.write(" ")
import csv
datawindow4 = height
with open("max y.csv", "w") as f:
    for d in datawindow4:
        f.write(str(d))
        f.write(" ")
import csv
datawindow4 = min_pos
with open("min x.csv", "w") as f:
    for d in datawindow4:
        f.write(str(d))
        f.write(" ")
import csv
datawindow4 = min_height*-1
with open("min y.csv", "w") as f:
    for d in datawindow4:
        f.write(str(d)) f.write(" ")
```
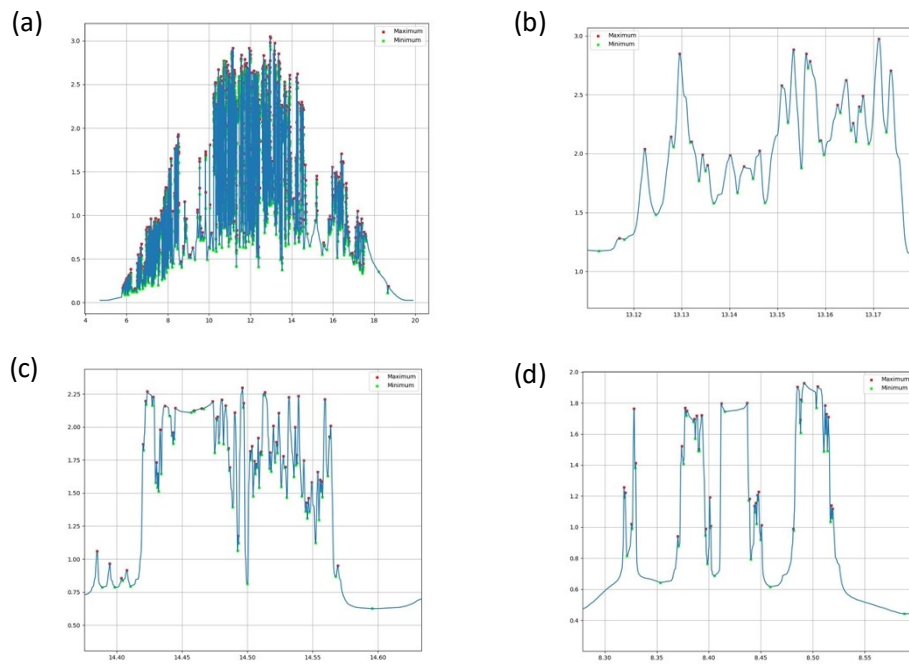
Fig. S_B9: Local maximums and minimums determination. (a) Full profile. (b) Zoomed area 1. (c) Zoomed area 2. (d) Zoomed area 3.

Obtained results can be seen on **Fig.S_B9**. As can be seen from zoomed randomly chosen areas (**Fig. S_B9b–d**), Python module is able to correctly detect all local minimums and maximums.

After detecting all local maximums and minimums, current ramps were defined as $\frac{\Delta I}{\Delta t}$ within each ramp up from minimum to maximum and ramp down from maximum to minimum. Obtained current ramps were distributed according to the frequency histogram (**Fig. S_B10**). As can be seen, high ramp rate events (from 0.5 to 3 A cm^{-2} s^{-1}) are present. Value of the current ramp of 1.5 A cm^{-2} s^{-1} was chosen as the reference for the accelerated stress test (AST) protocols step duration selection, in order to maximize possible triggers from a dynamic operation. Thus, AST conditions were chosen as cycling from 0 (minimal load in case of off-grid operation without a battery supply) to 3 A cm^{-2} (elevated load) with a step duration of 4 s.
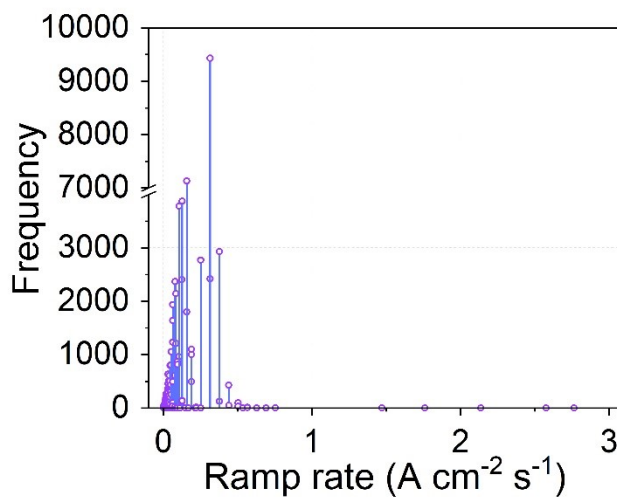

Fig. S_B10: Ramp rate frequency histogram.

References

1   G. Bender, M. Carmo, T. Smolinka, A. Gago, N. Danilovic, M. Mueller, F. Ganci, A. Fallisch, P. Lettenmeier, K. A. Friedrich, K. Ayers, B. Pivovar, J. Mergel and D. Stolten, *Int. J. Hydrogen Energy*, 2019, **44**, 9174–9187.

2   S. Al Shakhshir, X. Cui, S. Frensch and S. K. Kær, *Int. J. Hydrogen Energy*, 2017, **42**, 21597–21606.

3   J. O. Majasan, J. I. S. Cho, I. Dedigama, D. Tsaoulidis, P. Shearing and D. J. L. Brett, *Int. J. Hydrogen Energy*, 2018, **43**, 15659–15672.

4   F. Gutiérrez-Martín, L. Amodio and M. Pagano, *Int. J. Hydrogen Energy*, 2021, **46**, 29038–29048.

5   M. Müller, W. Zwaygardt, E. Rauls, M. Hehemann, S. Haas, L. Stolt, H. Janssen and M. Carmo, *Energies*, 2019, **12**, 4150.

6   R. E. Clarke, S. Giddey, F. T. Ciacchi, S. P. S. Badwal, B. Paul and J. Andrews, *Int. J. Hydrogen Energy*, 2009, **34**, 2531–2542.

7   Samsung SDI, SolarHub - PV Module Details: PV-MBA1BG255 - by Samsung SDI, https://solarhub.com/solarhub_products/34489-PV-MBA1BG255-Samsung-SDI, (accessed 21 October 2023).

8   Natural Resources Canada, High-Resolution Sol. Radiat. Datasets, https://www.nrcan.gc.ca/energy/renewable-electricity/solar-photovoltaic/18409, (accessed 21 October 2023).